Computational Condensed Matter 6 (2016) 5–17

Contents lists available at ScienceDirect

Computational Condensed Matter

journal homepage: http://ees.elsevier.com/cocom/default.asp

Understanding electronic and optical properties of La and Mn co-doped anatase TiO_2

Renhui Zhang [a, *], Juan Zhao [b], Yingchang Yang [a], Zhibin Lu [c], Wei Shi [a, **]

[a] Research Center of Material and Chemical Engineering, School of Material and Chemical Engineering, Tongren University, Tongren, 554300, PR China
[b] School of Mathematics and Information Science, Tongren University, Tongren, 554300, PR China
[c] State Key Laboratory of Solid Lubrication, Lanzhou Institute of Chemical Physics, Chinese Academy of Science, Lanzhou 730000, PR China

ARTICLE INFO

Article history:
Received 28 February 2016
Received in revised form
12 March 2016
Accepted 12 March 2016
Available online 15 March 2016

Keywords:
Electron
TiO_2
First-principles
Dipole moment

ABSTRACT

The electronic structures, dipole moment, and optical properties of La-doped, Mn-doped, and La-Mn-doped anatase TiO_2 have been investigated by means of GGA + U first-principles method, showing that the absorption coefficients of the La-Mn-doped TiO_2 under visible light to be sensitive to the doping positions of La and Mn atoms. La-Mn-TiO_2(1) exhibits the largest absorption coefficient in visible light because of the smallest band gap. Additionally, for the La and Mn co-doped TiO_2, the large dipole moment of TiO_6 octahedron is in prejudice of enhancing the optical responses under the visible light. We successfully probe the interesting optical response mechanism in this work.

1. Introduction

Due to the interesting demand for the environmental accountability and energy conversion [1], titanium dioxide (TiO_2) was continuously attracting substantial research in solar cells, lithium-ion batteries, purifying water, photolysis of water and optical degradation of organic compound [2–6] because of its strong oxidizing power, cost effectiveness, long term stability, and high catalytic activity [7,8]. However, it had large electronic band gaps of 3.0–3.2 eV [9], which limited its optical absorption in the ultraviolet (UV) region of the solar spectrum. However, the UV light only accounted for less than 5% of the entire solar energy [10]. Although TiO_2 was even efficient in utilizing the UV light, its overall solar activity was very limited. Furthermore, the photocatalytic activity depended on the amount of photo-exciting electrons and holes on the surface of the TiO_2 for the reaction. However, its photo quantum yield value was very low due to easily recombination of photo-exciting electron-hole pairs. Hence, it was highly desirable to develop TiO_2 with high catalytic activity under the visible light.

During the past few decades, tremendous effort has been devoted to the rational design of the better optical absorption of TiO_2 under visible-light region through the dopant of metal or non-metal. For instance, V doped TiO_2 photocatalyst prepared by the Klodek et al. exhibited excellent photocatalytic activity for photo-oxidation of ethanol [11]. Di Paola et al. reported that the transition metal doped TiO_2 samples have an effect on the photocatalytic degradation of organic compounds [12]. Meng et al. declared that N and transition metal co-doped TiO_2 exhibited superior photocatalytic activity under visible light. And they also pointed out the relationship between electronic structure and optical properties [13]. Ohno and Umebayashi et al. reported that S doped TiO_2 could improve the photocatalytic activity under visible-light irradiation [14–16]. Asahi and Maeda et al. prepared N doped TiO_2 films and found that they exhibit excellent photocatalytic activity under visible-light irradiation [17,18]. Indeed, the light absorption edge of the doped TiO_2 could be extended to the long wavelength range (mostly visible light range) with the help of these strategies. Unfortunately, the variable experimental conditions and sample preparation methods led to difficultly understanding their intrinsic activation mechanism. Luckily, the simulation method could well overcome the complexity of the experimental conditions and help us to analyze the microscopic information of electronic structure of the doped TiO_2, and understand the detailed effect of different doped elements and doped positions on the photocatalytic activity of TiO_2.

First-principles method provided a powerful tool to capture

* Corresponding author.
** Corresponding author.
E-mail addresses: zrh_111@126.com (R. Zhang), wlxsw@sina.cn (W. Shi).

http://dx.doi.org/10.1016/j.cocom.2016.03.001

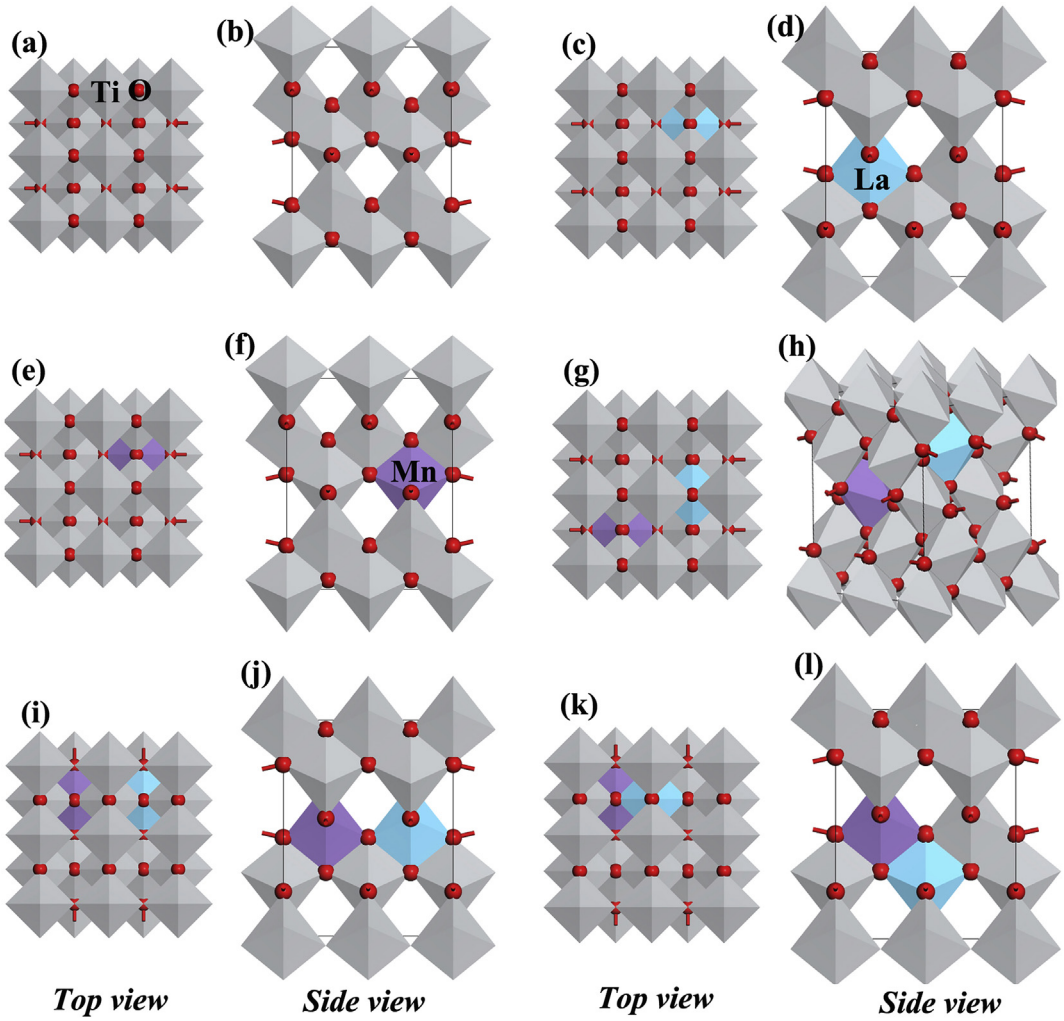

Fig. 1. Models of TiO_2 (a) top view, (b) side view, La-TiO_2 (c) top view, (d) side view, Mn-TiO_2 (e) top view, (f) side view, La + Mn-TiO_2(1) (g) top view, (h) side view, La + Mn-TiO_2(2) (i) top view, (j) side view, La + Mn-TiO_2(3) (k) top view, (l) side view.

atomic details and gained a deeper insight into the intrinsic activation mechanism of TiO_2 under visible light region. Yang et al. reported that the effect of N concentration on the formation energies and electronic band structure of N-doped TiO_2 has been investigated on the basis of first-principles calculations [19]. And Yang et al. also studied the photocatalytic activity of S and P doped TiO_2 under visible light from first-principles [20]. Weng et al. investigated the electronic structure and optical properties of the Co doped anatase TiO_2 based on the first-principles method [21]. Moreover, we have successfully probed the activation mechanism of C-N, N-La, and N-transition metal co-doped TiO_2 based on the first-principles method in our previous investigations [22–24]. Additionally, Li et al. [25–27]systematically investigated the band gap engineering of early transition-metal-doped anatase TiO_2, electronic, optical and photocatalytic behavior of Mn, N doped and co-doped TiO_2, and effects of oxygen vacancy on 3d transition-metal doped anatase TiO_2. Nowadays, more and more researchers payed attention to photo-activation mechanism of the anion or cation or anion and cation doped TiO_2 [28–30]. Lin et al. studied the photocatalytic performance of Mn and Fe codoped TiO_2 film [31], they found that two transition metals codoped TiO_2 improved synergistically the photocatalytic efficiency of TiO_2. A very limited number of investigations have considered the combined effect of using Mn and La as codopants. Also, we found that N-La, N-Mn co-doped TiO_2 exhibited excellent optical absorption under visible light, and La and Mn co-doped TiO_2 could improve its optical absorption under visible light.

Herein, we systematically investigate the electronic structure, dipole moment, electron localization function (ELF) and optical properties of La and Mn co-doped TiO_2 using GGA + U first-principles method, and try to probe the photo-activation mechanism of La and Mn co-doped TiO_2.

2. Computational method and details

Fig. 1a and b shows the top and side views of TiO_2 respectively. Fig. 1c–f shows the top and side views of La or Mn mono-doped TiO_2. Ti atom is replaced by La or Mn atom, the atom fraction is 6.67%. The top and side views of La and Mn co-doped TiO_2 is plotted in Fig. 1g–l, Ti atoms are replaced by La and Mn atoms, the atom fraction is 13.3%. La and Mn co-doped TiO_2 are marked as La + Mn-TiO_2(1), La + Mn-TiO_2(2), La + Mn-TiO_2(3) in the work. The pseudo atomic calculations perform for La $5s^25p^65d^16s^24f^0$, Mn $3d^54s^2$, O $2s^22p^4$, Ti $3s^23p^63d^24s^2$.

The first-principles calculations are performed using the CASTEP module in Materials Studio 6.0. The energy plane-wave pseudopotential total calculation method is carried out for all the calculations based on the density functional theory. The generalized-

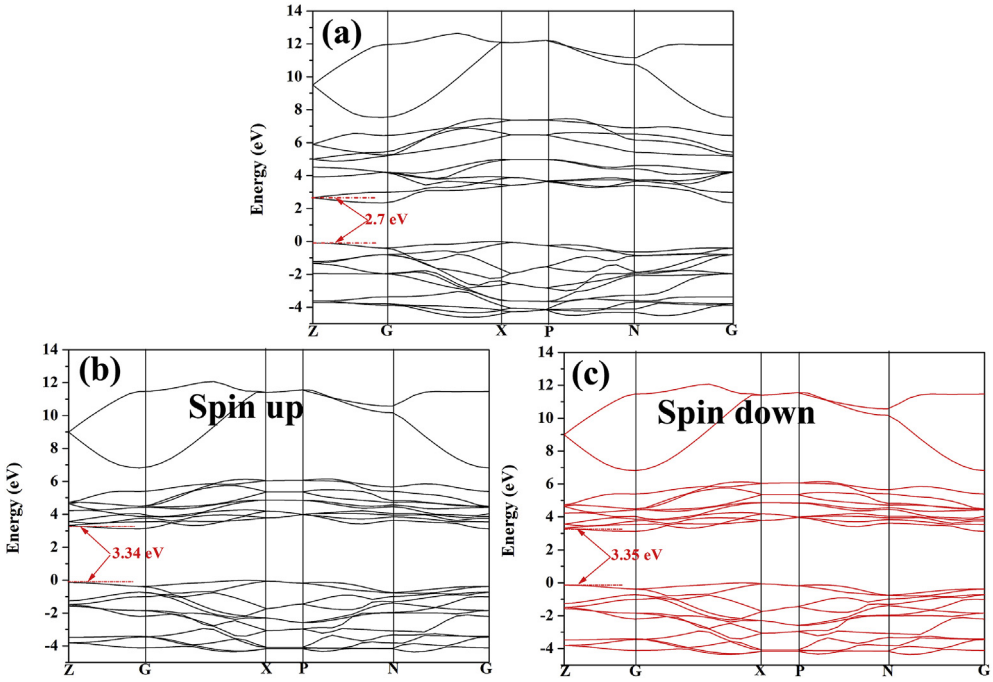

Fig. 2. Band structures of TiO_2 (a) GGA method, (b) and (c) GGA + U method.

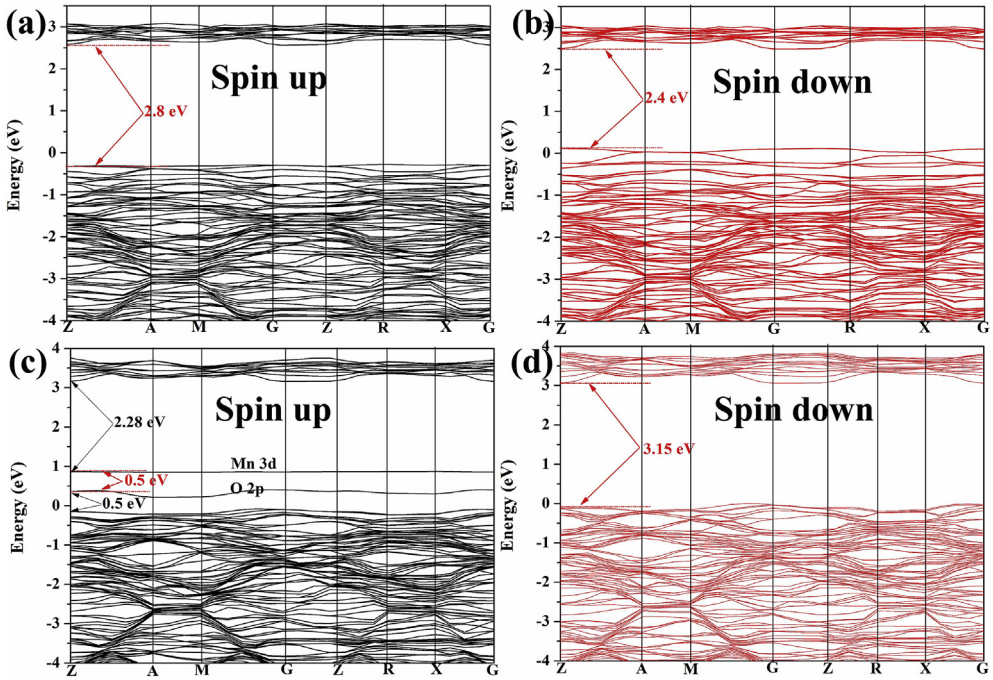

Fig. 3. Band structures of (a) and (b) La or (c) and (d) Mn doped TiO_2 based on GGA + U method.

gradient approximation (GGA) with the Perdew-Burke-Ernzerhof exchange-correlation functional is performed for all the calculations [32]. Interaction between the valence electrons and ion core is substituted by an ultrasoft pseudopotential. A plane-wave cutoff energy is 350 eV. The Monkhorst-Park scheme K-point grid is set as $4 \times 4 \times 5$ for all models. Spin-polarization is performed for all the structural optimizations. Geometric relaxation is obtained with the Broyden-Fletcher-Goldfarb-Shanno (BFGS) algorithm until the atomic forces are smaller than 0.03 eV/Å. The convergence threshold for self-consistent iterations is set as 1×10^{-6} eV. After the equilibrium lattice constants are determined, the volume and shape of the models remain unchanged. In the geometry optimization, the energy change, maximum force, maximum stress and maximum displacement tolerance are set to 1×10^{-5} eV/atom, 0.03 eV/Å, 0.05 GPa, and 0.001 Å. In addition, the GGA + U method is adopted to describe the strong on-site Coulomb repulsion in order to accurately describe the electronic structures. We have considered an on-site Coulomb repulsion on the Ti 3d states, and

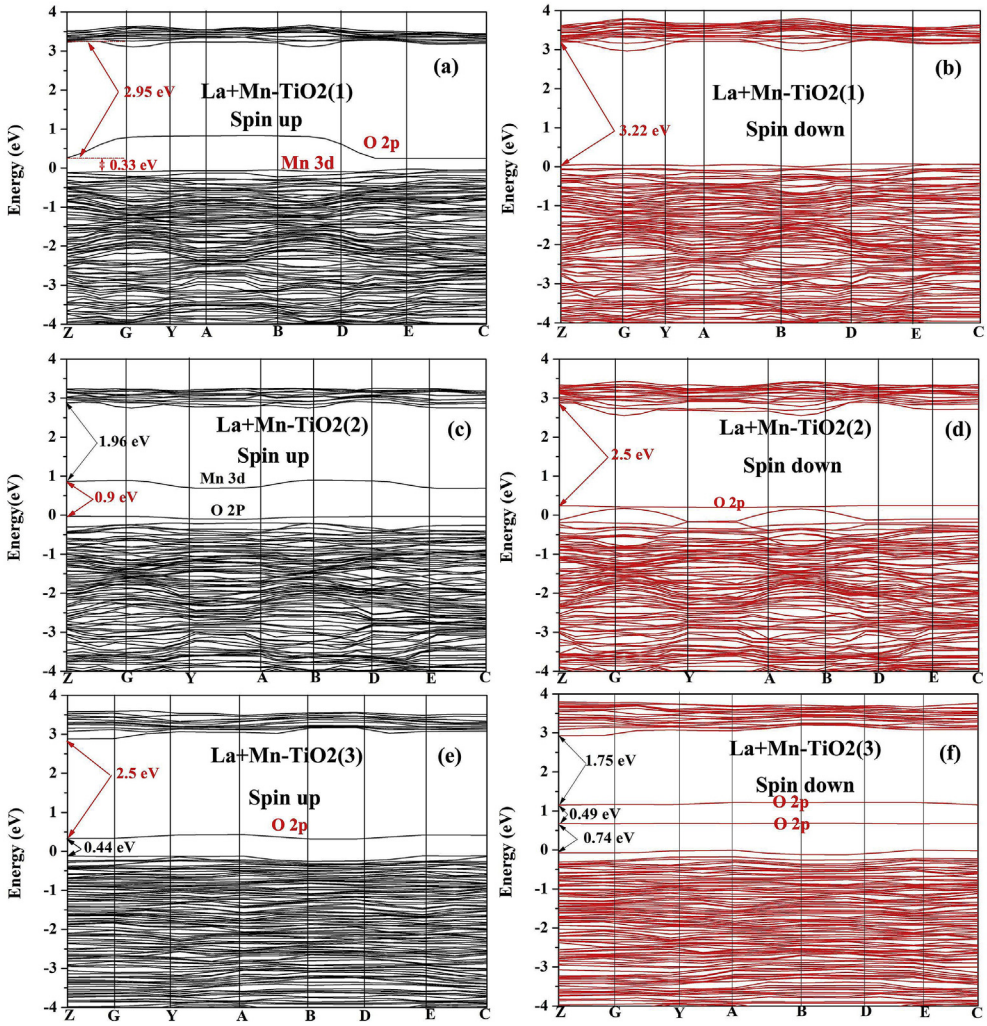

Fig. 4. Band structures of (a)–(f) La and Mn co-doped TiO_2 based on GGA + U method.

Mn 3d states using $U_{Ti} = 7.8$ eV [33], $U_{Mn} = 9.0$ eV [13], and $J = 1$ eV. Additionally, $U = 7.5$ eV is used to shift the unoccupied La f states to higher energies. However, because of the localized nature of the f states, it does not influence qualitatively the electronic behavior of the system [34], thus, the effect of the f states of La on the electronic properties do not be considered in this paper. Mulliken population analysis is selected to analyze the average net charge. In order to obtain the accurate results, the crystal structures and atomic co-ordinates are optimized firstly under the principle of energy minimization, and the appropriate cell parameters are obtained. Subsequently, we calculate the band structure, density of states, ELF, optical properties of the doped systems based on the GGA + U method. After geometrical optimizations, the lattice parameters of pure anatase TiO_2 are as follows, $a = b = 3.7973$ Å, $c = 9.7851$ Å. The calculated results are well in consistent with the experimental values, $a = b = 3.7848$ Å, $c = 9.5124$ Å [35]. It reveals that the calculation methods are reasonable and the calculation results are authentic.

3. Results

3.1. Band structure

As we known, the band gap values are determined by the valence band and conduction band, and the impurity states in the band gaps can reduce the electronic transition energy of specimen. Based on this view, the band gap of doped TiO2 is well investigated. For a comparison, the band structure of the undoped TiO_2 is plotted in Fig. 2a–c. Fig. 2a shows that the band structure of undoped TiO_2 displays a direct band gap about 2.7 eV calculated by the GGA method. Fig. 2b and c also reveals a direct band gap about 3.34 eV calculated by the GGA + U method, which indicates that the band gap calculated by the GGA + U method is in consistent with the experimental value (3.2 eV) [9]. Subsequently, the GGA + U method is carried out to ensure the accuracy of the calculated results. The band structure of La or Mn doped TiO_2, La and Mn co-doped TiO_2 is plotted in Fig. 3 and 4. Fig. 3a and b shows the spin-up/-down band structure of La doped TiO_2, which reveals that the 2p down spin of O states is conducive to reducing the band gap. The spin-up/down band structure of Mn doped TiO_2 plotted in Fig. 3c and d indicates that the 3d/2p up spin of Mn and O states is helpful for decreasing the band gap. And the band gap of Mn doped TiO_2 is decreased to the value of 0.5 eV Fig. 4 displays the spin-up/down band structure of La and Mn co-doped TiO_2. Fig. 4a and b represents the spin-up/down band structure of La-Mn-TiO_2(1). Fig. 4a shows that one impurity energy level located in the band gap is conducive to decreasing the band gap. And the Mn 3d states shift downward by the value of 2.95 eV. There are no impurity energy levels in the

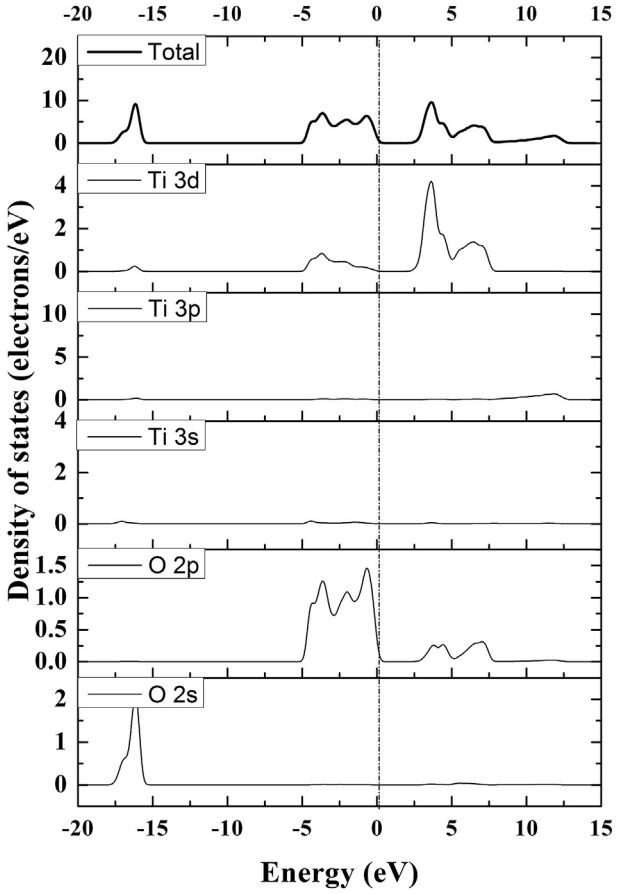

Fig. 5. Total and partial density of states of TiO_2 calculated using GGA method.

forbidden band as shown in Fig. 4b. Combining with Fig. 4a and b, the band gap is decreased to the value of 0.33 eV. The spin-up/down band structure of La-Mn-TiO_2(2) is plotted in Fig. 4c and d. Two impurity energy levels are found, one lies on the top of the Femi level, the other one closes to the Femi level, which are helpful for decreasing the band gap. The band gap is reduced to the value of less than 0.9 eV Fig. 4e and f shows the spin-up/down band structure of La-Mn-TiO_2(3). It can be seen from Fig. 4e and f that 2p down spin of O states is observed over the Femi level, and 2p up spin of O states are found in the band gap.

3.2. Density of states

In order to further analyze the composition of valence band (VB) and conduction band (CB) and well understand the changes of the electronic structures, the total density of states (TDOS) and partial density of states (PDOS) of TiO_2 calculated by the GGA method is shown in Fig. 5. The VB mainly consists of Ti 3d, O 2s, and O 2p states. O 2p and Ti 3d states are major composition for the VB. For comparison, the TDOS and PDOS of TiO_2 (Fig. 6) are calculated by the GGA + U method. The VB also mainly consists of Ti 3d, O 2s and O 2p states. The CB also consists of O 2p and Ti 3d states. Interestingly, the Ti 3d states move up from 3.5 eV to 3.8 eV and the O 2p states shift from −0.6 eV to −0.8 eV compared to Fig. 5. Fig. 7 displays the TDOS (Fig. 7a) and PDOS (Fig. 7b–e) of La doped TiO_2 calculated by the GGA + U method. Fig. 7b–e shows that the VB is comprised of La 5p, La 5d, O 2s, O 2p, Ti 3s and Ti 3d states, the CB mainly consists of Ti 3d state. Fig. 7c and e displays the PDOS of O atoms (O near La/Ti atom). Fig. 7c shows the PDOS of 2p/2s up and down spin of O states that exhibits the symmetrical distribution. Some La 5d states sufficiently disperse within the O 2p states indicating the covalent property of the La–O bond. The PDOS of La 5d states displays the symmetrical distribution leading to the same

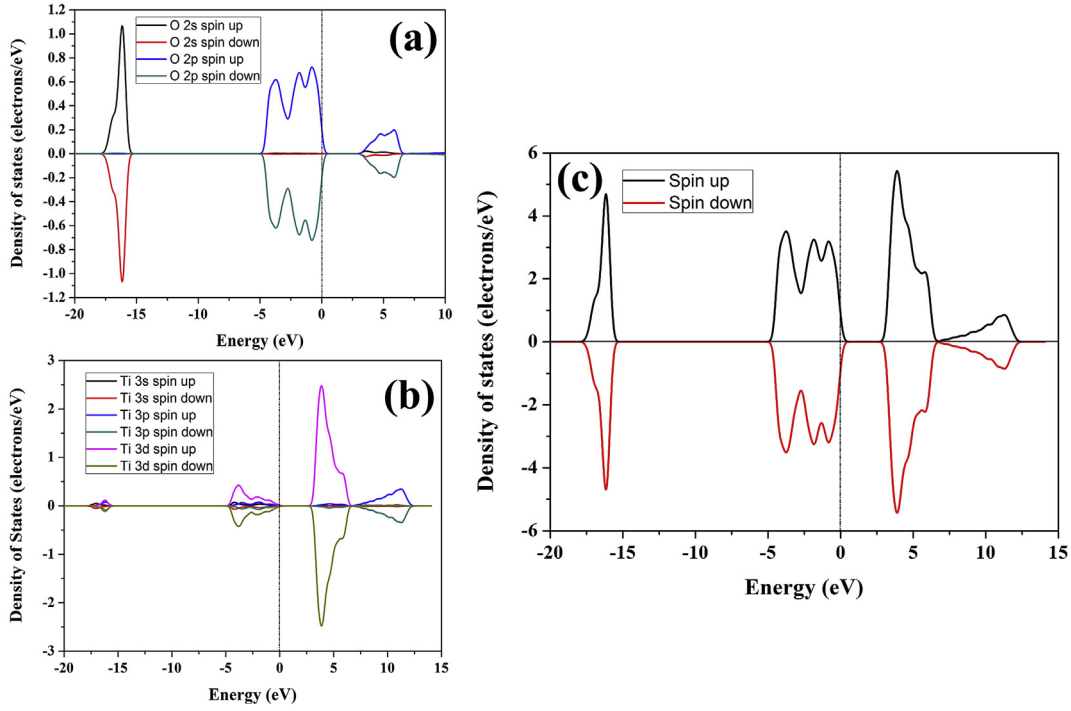

Fig. 6. (a) and (b) Partial density of states of TiO_2, (c) Total density of states of TiO_2 calculated using GGA + U method.

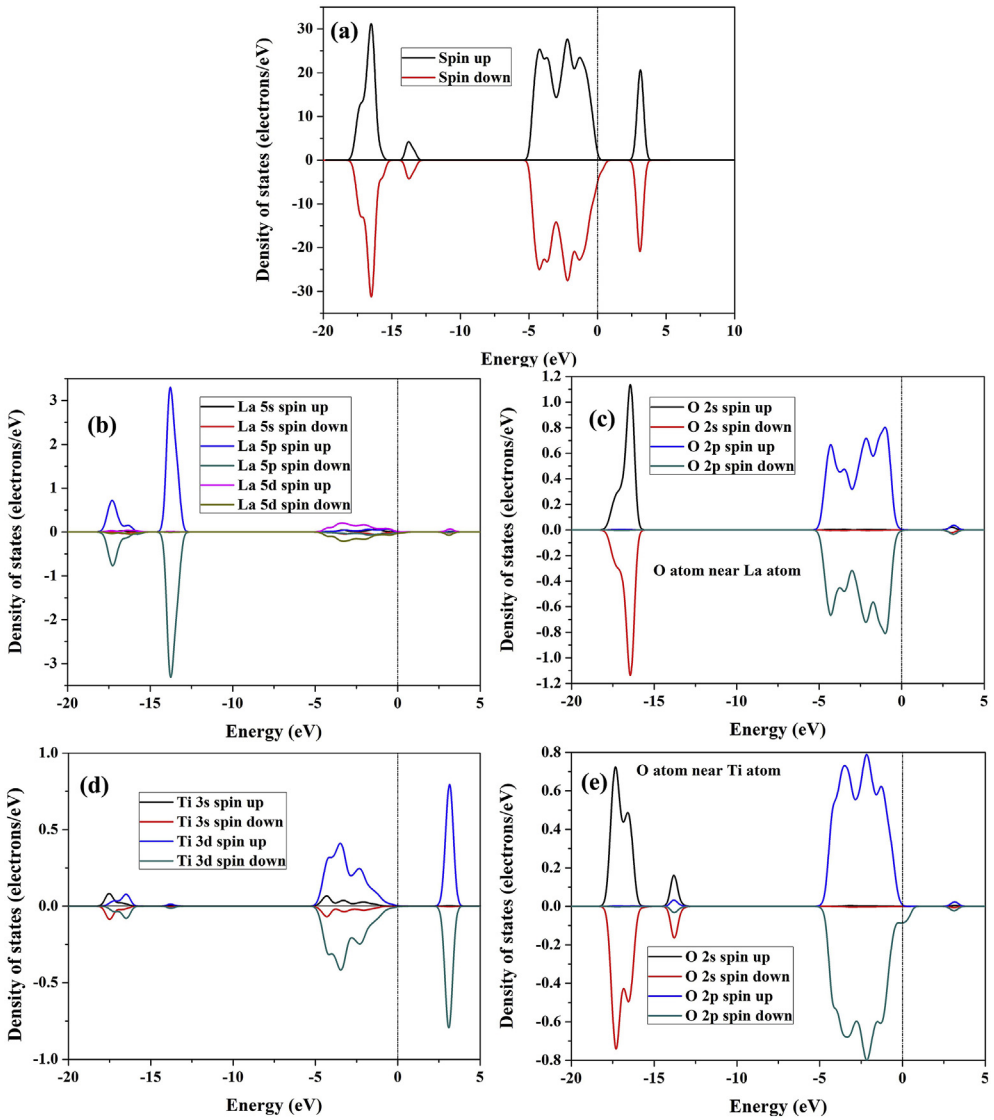

Fig. 7. Total and partial density of states of La doped TiO_2 calculated using GGA + U method.

distribution of the O atom (O near La atom). It indicates that the doped La almost does not impact on the location of the O 2p and Ti 3d states [33]. However, the PDOS of 2p/2s up and down spin of O states obviously exhibits the variable distribution as shown in Fig. 7e. The TDOS and PDOS of Mn doped TiO_2 is plotted in Fig. 8. Fig. 8a shows that the upper valence band is dominantly composed of O 2p states, Ti 3d states, Mn 3d states. Additionally, Fig. 8b illustrates that the spin-up orbitals of Mn 3d states are obviously stronger than those of spin-down ones. The similar phenomenon is also observed in Fig. 8c and d, which reveals that the doped Mn has an effect on the distribution of O 2p (O near Mn atom) and Ti 3d states. Incorporation of Mn into TiO_2 also influences the location of O 2p (O near Ti atom) and Ti 3d states as shown in Fig. 8e. According to the above analysis, we can therefore conclude that the doped Mn has a significant effect on the location of O 2p and Ti 3d states. Fig. 9a presents the TDOS of La + Mn-TiO_2(1). Fig. 9b–g shows the PDOS of La, O (O near La atom), Mn, O (O near Mn atom), Ti, O (O near Ti atom). Combining with Fig. 9b and c, the changes of O 2s, O 2p (O near Mn atom), Ti 3s, Ti 3p, Ti 3d, O 2s, O 2p (O near Ti atom) could be attributed to the incorporation of Mn into TiO_2. The TDOS of La-Mn-TiO_2(2) is shown in Fig. 10a. Fig. 10b–g displays the PDOS of La, O (O near La atom), Mn, O (O near Mn atom), Ti, O (O near Ti atom). The location of La states shows the symmetrical distribution as shown in Fig. 10b. The La 5d, Mn 3d and Ti 3d states are plotted in Fig. 10b, d, and f, as well as the O 2p states that can possibly hybridize with d electrons (Fig. 10c, e, and g). The TDOS (Fig. 11a) and PDOS (Fig. 11b–g) are displayed for La-Mn-TiO_2(3) calculated by the GGA + U method. Fig. 11b shows that the PDOS of La exhibits the symmetrical distribution. However, the PDOS of O 2s, O 2p of O atom (O near La atom) shows the different characteristics as shown in Fig. 11c. The PDOS of Mn, O (O near Mn atom), Ti, O (O near Ti atom) also shows the variable characteristics compared to the PDOS of La (Fig. 11d–g).

3.3. Electron localization function

The electron localization function (ELF) analyses are selected to investigate the evolution of the bonding structure of the doped systems. ELF is a position-dependent function that the value varies in the range of 0–1. When ELF = 1.0, which corresponds to covalent bonding. ELF = 0.5 corresponds to electron/gas-like pair probability, which is an indication of metallic bonding. And for ELF <0.5, the

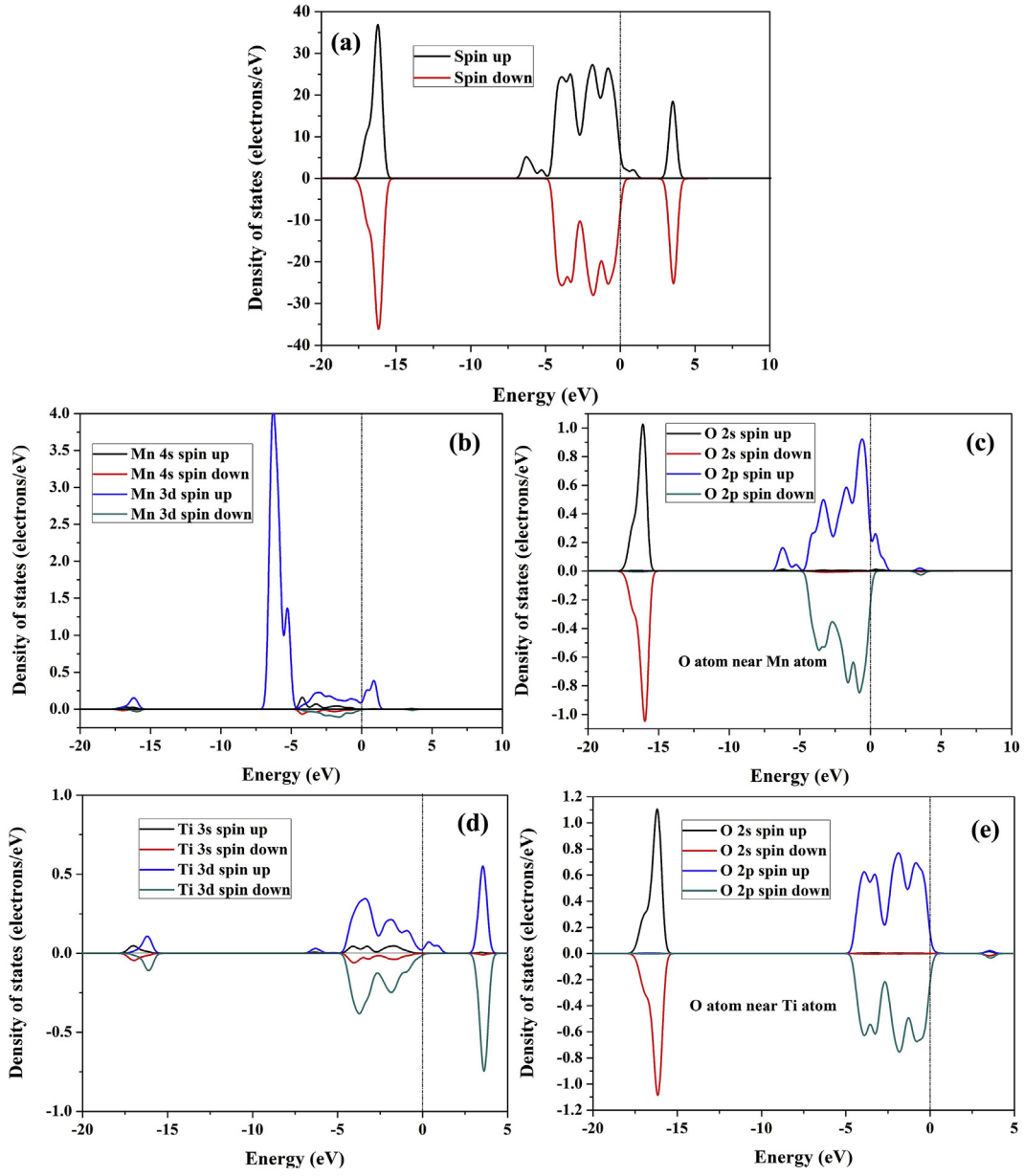

Fig. 8. Total and partial density of states of Mn doped TiO_2 calculated using GGA + U method.

function is undefined [36–38], which would imply that these atoms do not interact with anything in the unit cell. The ELF plots of the TiO_2 and doped TiO_2 are appeared in Fig. 12. Compared with Fig. 12a and b, the decrease of ELF is observed. For La doped TiO_2 (Fig. 12c), the covalent bonding is clearly visible in locations where ELF ~0.9 between the La and O atoms. Fig. 12d shows the ELF plots of Mn doped TiO_2. The absence of any type of chemical bonding (covalent, metallic or ionic) is apparent near the Mn atom where ELF ~ 0. For La-Mn-TiO_2(1) (Fig. 12e and f), La exhibits a covalent character in locations where ELF ~0.9. Mn displays the absence of any type of chemical bonding. Fig. 12g shows the ELF plots of La-Mn-TiO_2(2). La also reveals a covalent character in locations where ELF ~0.9. The value of ELF is about zero near the Mn atom, indicating the absence of any type of chemical bonding. Fig. 12h shows the ELF plots of La-Mn-TiO_2(3). Both La and Mn exhibits the absence of any type of chemical bonding in locations where ELF ~0.

3.4. Diploe moment

The optical properties of a semiconductor are mostly decided by its electronic structures. The changes of bond length and atomic charge lead to the center of gravity of negative charges deviating from the position of Ti^{4+} ion in TiO_6 octahedron. And then the dipole moment would be non-zero. In our previous investigations [22,23], we successfully probe the relationship between the dipole moment and optical properties of C-N-doped and N-La-doped anatase TiO_2, which would help us to well improve the visible-light absorption of the anatase TiO_2. The calculated TiO_6 dipole moment is obtained by the dipole moment formula ($\mu = qr$, where q is the net charge, and r is the distance between the center of O and Ti atom) [39]. The calculated results are listed in Table 1.

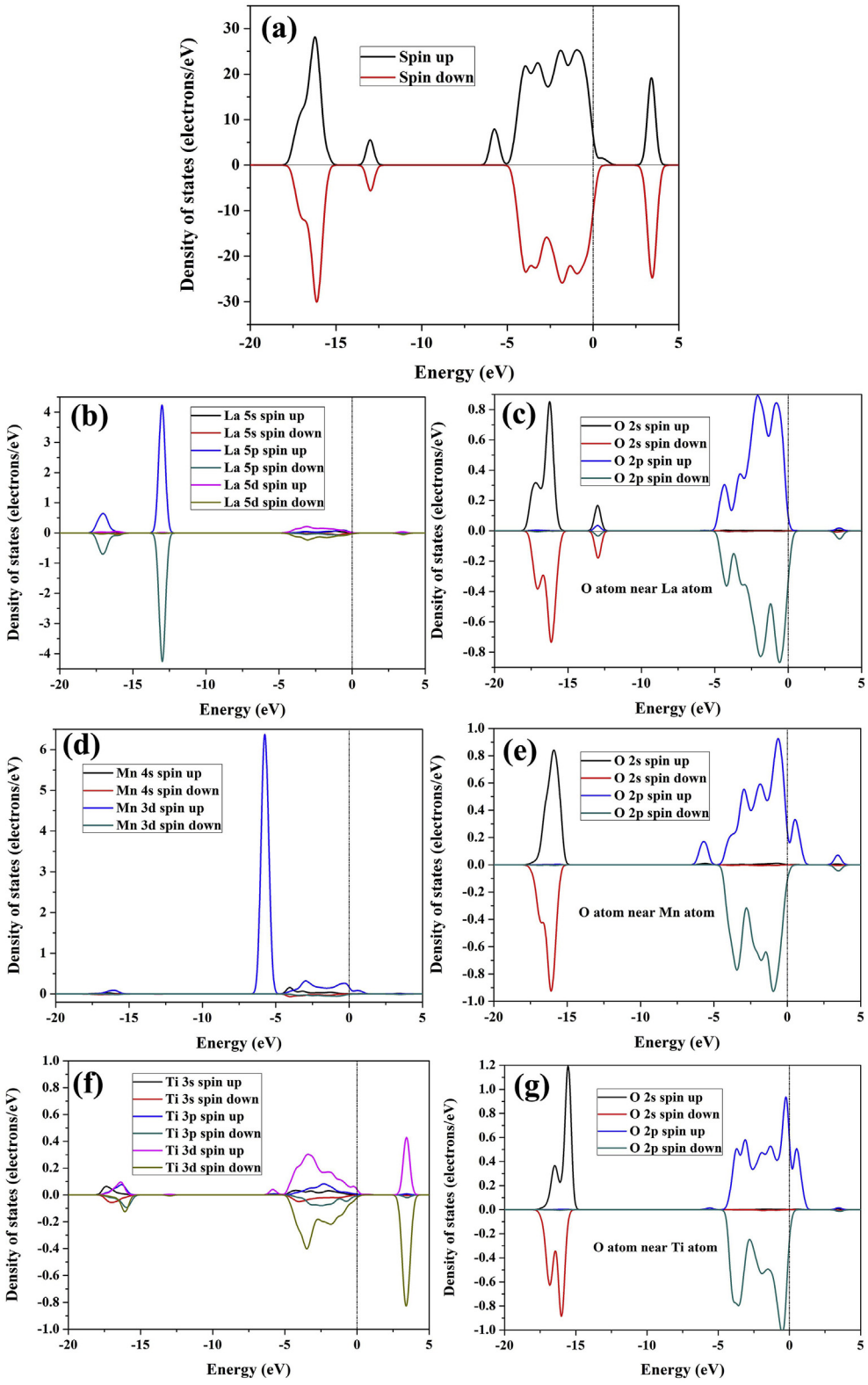

Fig. 9. Total and partial density of states of La + Mn-TiO_2(1) calculated using GGA + U method.

3.5. Optical properties

We also evaluate the optical absorption spectra for the TiO_2 and doped TiO_2. The calculated optical absorption spectra are shown in Fig. 13. Obviously, either GGA or GGA + U method is used to simulate the optical properties of TiO_2, it absorbs mainly UV light and a very weak absorption in the visible-light region is observed in Fig. 13, which is in consistent with the Ref. [22,40]. During introducing dopants, the absorption edges extend beyond the UV light regime. For La, Mn mono-doped or La and Mn co-doped TiO_2, the

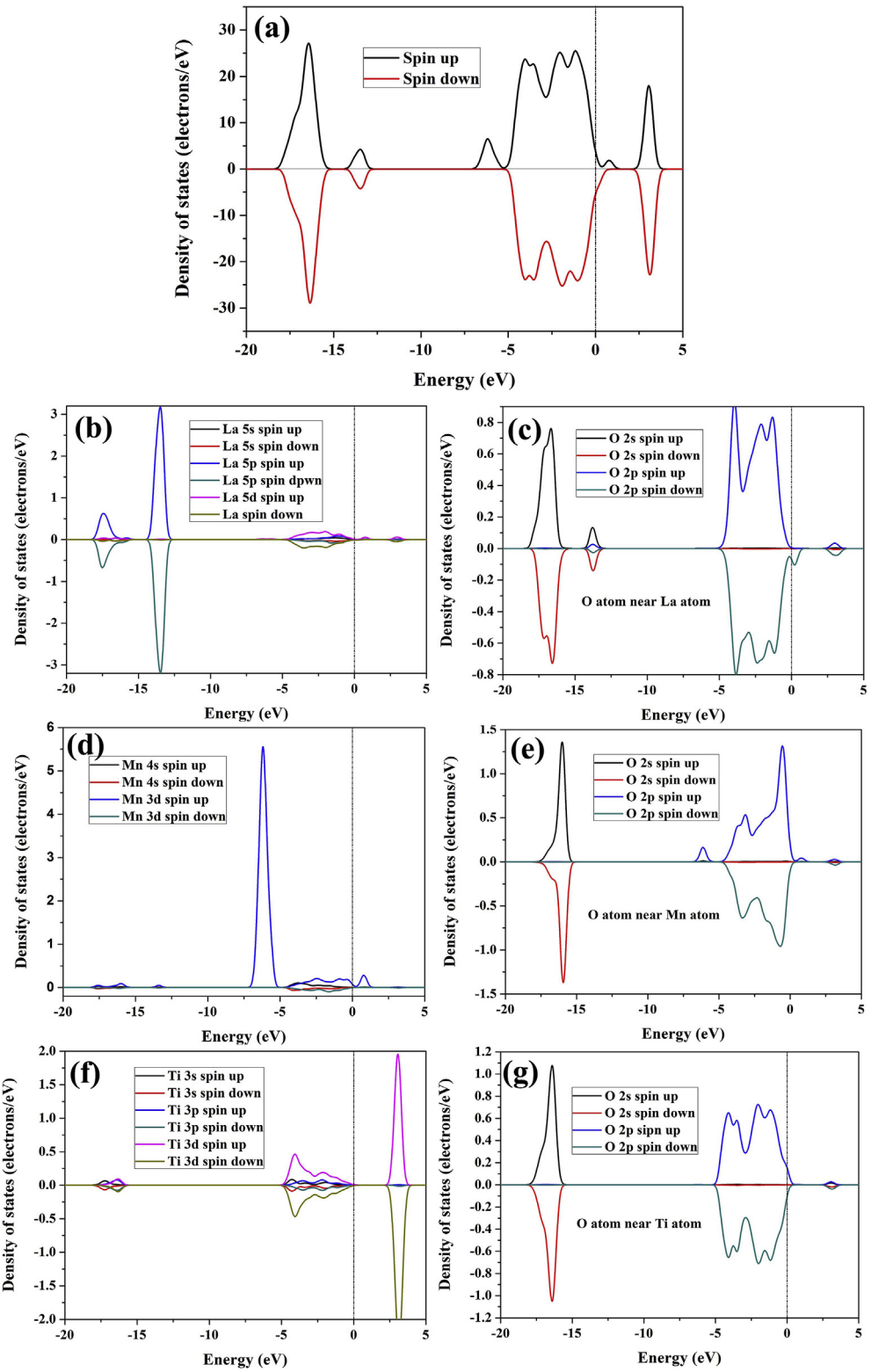

Fig. 10. Total and partial density of states of La-Mn-TiO_2(2) calculated using GGA + U method.

optical properties in the wavelength range less than 400 nm are controlled by the electronic transitions between O 2p states and Ti 3d states [13]. Therefore, the spectra are nearly identical in this wavelength range. In contrast, the optical properties in the wavelength range of more than 400 nm are different, which are affected by the transitions involving the impurity states. Clearly, the anatase TiO_2 is visible-light responsive upon La and Mn co-doping, and the absorption strength in the visible spectrum and even in the infrared range is improved when the La and Mn atoms replace Ti atoms. Combining with Fig. 13 and Table 1, we can therefore conclude that

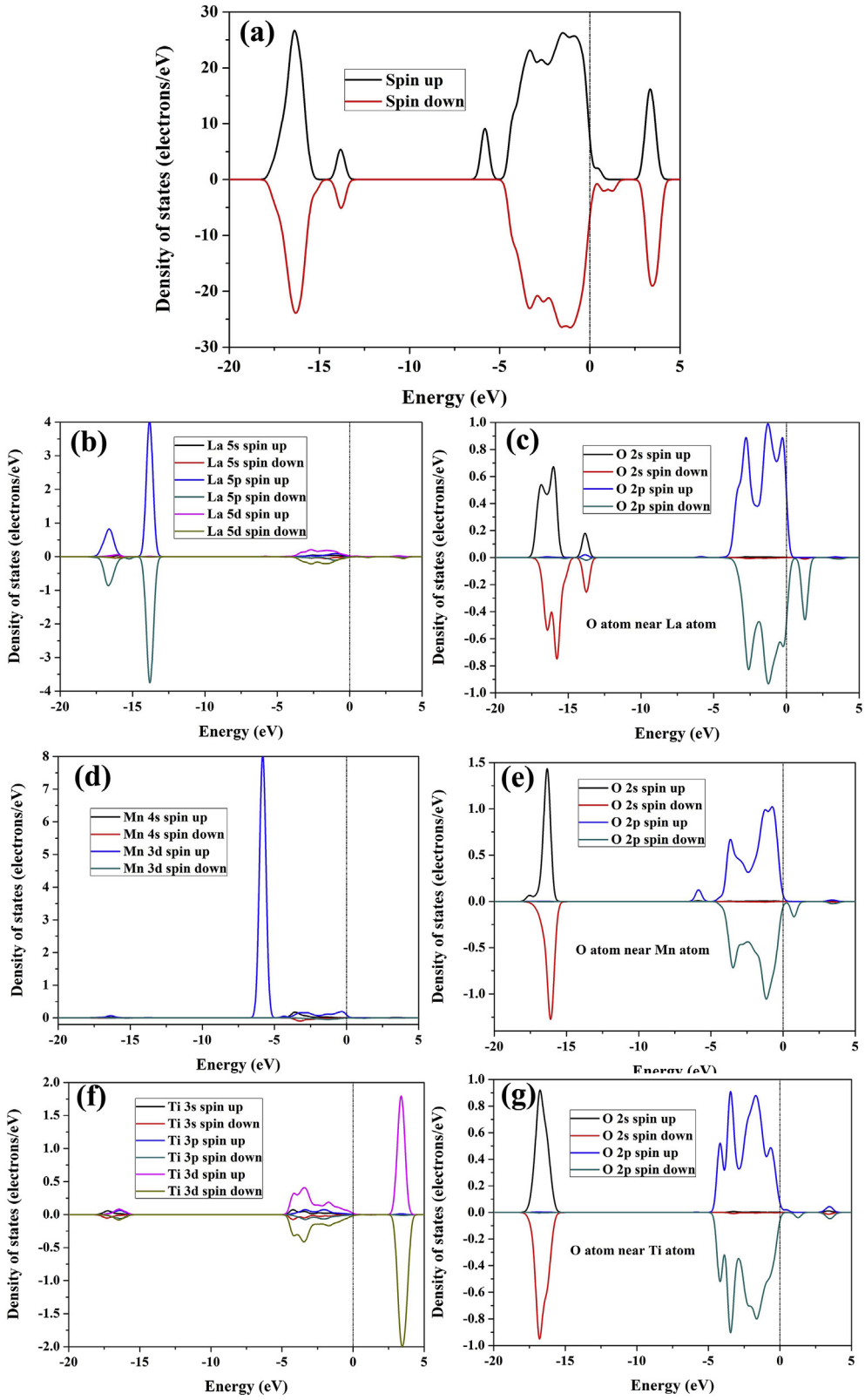

Fig. 11. Total and partial density of states of La-Mn-TiO_2(3) calculated using GGA + U method.

the lowest value of dipole moment corresponds to the superior optical absorption coefficient under visible-light region for La and Mn co-doped TiO_2.

4. Discussion

Three principal results pertaining to the optical properties of doped anatase TiO_2 have arisen from the observations investigated

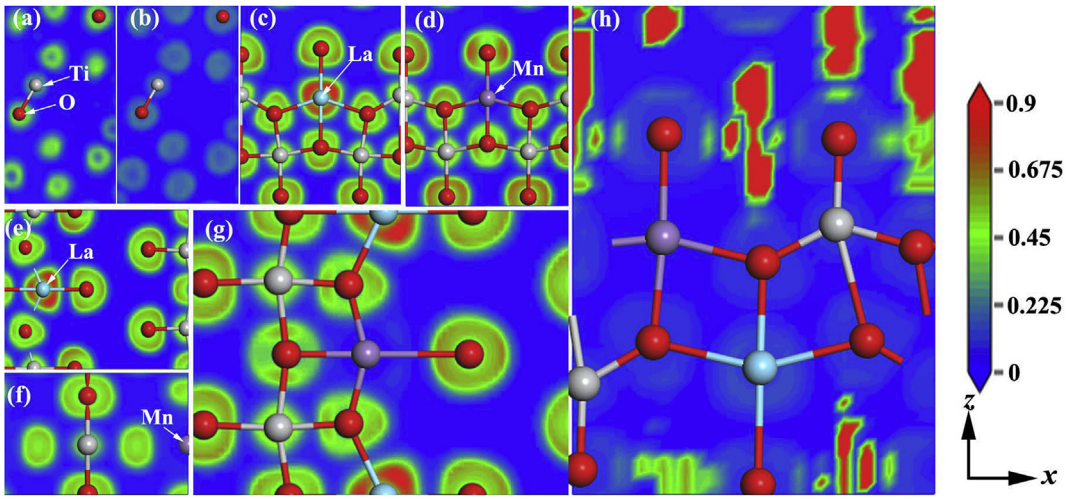

Fig. 12. Electron localization function of (a) TiO_2, (b) TiO_2 + U, (c) La doped TiO_2, (d) Mn doped TiO_2, (e) and (f) La-Mn-TiO_2(1), (g) La-Mn-TiO_2(2), (h) La-Mn-TiO_2(3) based on GGA + U method.

Table 1
The average bond length, net charges, dipole moment of deficient cation doped TiO_2 after geometry optimization.

Samples	Bond length(Å)			Net charge (eV)				Dipole moment (D)
	Ti–O	La–O	Mn–O	Ti	O	La	Mn	
TiO_2	2.079	–	–	1.33	−0.67	–	–	1.384
TiO_2 + U	2.011	–	–	1.47	−0.73	–	–	1.488
La-TiO_2	1.983	2.400	–	1.33	−0.73	2.8	–	1.189
Mn-TiO_2	1.984	–	2.106	1.47	−0.72	–	2.35	1.488
La-Mn-TiO_2(1)	1.972	2.325	2.182	1.37	−0.71	2.62	1.09	1.301
La-Mn-TiO_2(2)	2.007	2.408	2.098	1.32	−0.62	2.72	1.04	1.405
La-Mn-TiO_2(3)	2.094	2.504	2.365	1.37	−0.63	2.37	1.07	1.549

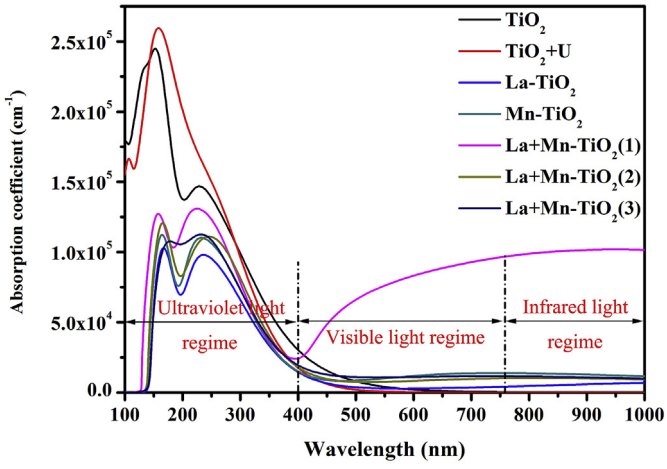

Fig. 13. The calculated optical properties for the variable samples.

in Section 3. The first is that the largest dipole moment does not correspond to the superior optical absorption under visible-light region. And the second is that the GGA + U method has a significant effect on the distribution of the DOS of the doped anatase TiO_2, and impacts the style of the chemical bond. And the last is that the optical absorption in the visible-light region of La and Mn co-doped anatase TiO_2 is closely related to the doped positions of La and Mn atoms. The interesting results are well discussed as follows.

Sato et al. reported that the dipole moment of the distorted octahedral could well promote the charge separation in the initial process of the photoexcitation and be useful for enhancing the photocatalytic activity [41]. And Sato et al. also declared that the dipole moment was beneficial to separation of photoexcited electrons and holes, which were conducive to enhancing the photocatalytic activity [42]. Chen et al. reported that the excited electrons and holes may separate from each other and migrate to the surface to perform photocatalytic reactions during the photocatalytic process. During the electrons and holes separation and migration processes, some of the excited electrons and holes may recombine and disappear [10,43–45]. They also declared that the photocatalytic activity depended on the amount of working electrons and holes on the surface of the photocatalyst for the reaction. In this work, we find that the largest dipole moment is not conducive to improving the optical absorption in the visible-light region, which may be attributed to the recombination of the excited electrons and holes leading to the decrease of the amount of working electrons and holes.

La-Mn-TiO_2(3) exhibits the largest dipole moment, but a smaller optical absorption coefficient in the visible-light region. The DOS of La-Mn-TiO_2(3) plotted in Fig. 11 reveals that the PDOS of O atom located near La, Mn and Ti atoms shows obviously spin-polarized phenomenon. Fig. 12 shows that the chemical bond styles between La, Mn, Ti and O atoms are undefined, O and O atoms obviously tend to be covalent bonds due to ELF ~ 0.9. Chen et al. reported that the doped La almost does not impact on the location of the O 2p and Ti 3d states [33]. Indeed, the La has no effect on the location of the O 2p and Ti 3d states in this work. Nevertheless, the doped Mn has a significant effect on the location of the O 2p and Ti 3d states, which further impacts the chemical bond styles. In

addition, the largest dipole moment generally corresponds to the large lattice distortion, which would hinder photoactivity [31].

Additionally, Fig. 1g–l shows the models of the La and Mn co-doped anatase TiO_2. The dopant of La and Mn atom shows the different doped positions, corresponding to the variable optical absorption coefficient as shown in Fig. 13. Generally, the optical properties are closely related to the band gap of the semiconductor [46–49]. Indeed, in this work, the smallest band gap corresponds to the superior optical absorption coefficient in visible-light region. Wei et al. reported that non-metal and metal element doped $SrTiO_3$ could keep charge balance [50]. And thus the photocatalytic activity under visible light could be improved to an extensive degree. However, in this work, the La, Mn atoms could release one more electron than Ti atom to the TiO_2 lattice and may be as a single donor. The extra electron brought by La and Mn dopant would be lone pair electrons due to the lack of the unpaired non-metal 2p electrons. Spontaneously, the charge balance would be hardly achieved. Combining with Figs. 7 and 8, the introduction of La or Mn atom leads to the O 2p valence band suffering a further expansion. La related states have few contributions neither to the VB nor to the CB because of the ionic interaction between La and TiO_6 [42], while Mn 3d states have some contributions to the CB. O 2p states have some contributions to the VB. Compared to Fig. 6, O 2p states shifts from the VB to CB and Mn 3d states move downward near the Femi level, which leads to the decrease of the band gap. In Fig. 4a and b, the band gap (0.33 eV) of La-Mn-TiO_2(1) could be calculated by the deviation between O 2p and Mn 3d states. Fig. 4c and d shows that the band gap is less than 0.9 eV for La-Mn-TiO_2(2). In Fig. 4e and f, the 2p up spin of O states and 2p down spin of O states are found in the forbidden band. The band gap of La-Mn-TiO_2(3) should be calculated between O 2p and Ti 3d states. The value of the band gap is 1.75 eV. According to the above discussion, the charge balance initially tends to be hardly achieved, however, the charge balance could be obtained in theory by the GGA + U method that could impact the distribution of the DOS of La and Mn co-doped TiO_2. Indeed, the doped positions of La and Mn atoms have a significant effect on the electronic structures of La and Mn co-doped anatase TiO_2 as shown in Figs. 9–11. Then the variable electronic structures could impact the value of the band gap. As a result, the optical absorption coefficient under visible light can be improved to an extensive degree due to a low band gap value and the theoretical charge balance.

5. Conclusions

The electronic and optical properties of La/Mn mono-doped, and La-Mn-doped anatase TiO_2 have been investigated by means of GGA + U first-principles calculations. The results indicate that the optimal doping model is La-Mn-TiO_2(1) that possesses energetic and high optical absorption coefficient under visible light. For this two cations co-doped TiO_2 system, the La related states have few contributions neither to the VB nor to the CB, however, the Mn and O related states exhibit more contributions to the VB and CB. Additionally, the doped positions of La and Mn atoms are closely related to the optical absorption coefficient under visible light due to influence of the distribution of Mn and O related states in the band gap. This work opens a new way to improve the optical absorption coefficient under visible light.

Author contribution

Renhui Zhang and Juan Zhao equally contribute to this paper. Renhui Zhang and Juan Zhao carried out for the first principles calculations. And all author reviews the paper carefully.

Acknowledgments

This work is supported by the Doctor Foundation of Tongren University (Grant no. trxyDH1515).

References

[1] Y. Yan, H. Guan, S. Liu, R. Jiang, Ag3PO4/Fe2O3 composite photocatalysts with an n–n heterojunction semiconductor structure under visible-light irradiation, Ceram. Int. 40 (2014) 9095–9100.
[2] Y. Yang, X. Ji, M. Jing, H. Hou, Y. Zhu, L. Fang, X. Yang, Q. Chen, C.E. Banks, Carbon dots supported upon N-doped TiO_2 nanorods applied into sodium and lithium ion batteries, J. Mater. Chem. A 3 (2015) 5648–5655.
[3] Z. Li, Y. Zhu, F. Pang, H. Liu, X. Gao, W. Ou, J. Liu, X. Wang, X. Cheng, Y. Zhang, Synthesis of N doped and N, S co-doped 3D TiO2 hollow spheres with enhanced photocatalytic efficiency under nature sunlight, Ceram. Int. 41 (2015) 10063–10069.
[4] I.H. Chowdhury, S. Ghosh, M.K. Naskar, Aqueous-based synthesis of mesoporous TiO2 and Ag–TiO2 nanopowders for efficient photodegradation of methylene blue, Ceram. Int. 42 (2016) 2488–2496.
[5] W.L. Wang, J.-Y. Park, V.H. Nguyen, E.M. Jin, H.-B. Gu, Hierarchical mesoporous rutile TiO2/C composite nanospheres as lithium-ion battery anode materials, Ceram. Int. 42 (2016) 598–606.
[6] H. He, Y. Miao, Y. Du, J. Zhao, Y. Liu, P. Yang, Ag2O nanoparticle-decorated TiO2 nanobelts for improved photocatalytic performance, Ceram. Int. 42 (2016) 97–102.
[7] P.S. Saud, B. Pant, M. Park, S.-H. Chae, S.-J. Park, M. Ei-Newehy, S.S. Al-Deyab, H.-Y. Kim, Preparation and photocatalytic activity of fly ash incorporated TiO2 nanofibers for effective removal of organic pollutants, Ceram. Int. 41 (2015) 1771–1777.
[8] Z.A. Lin, W.C. Lu, C.Y. Wu, K.S. Chang, Facile fabrication and tuning of TiO2 nanoarchitectured morphology using magnetron sputtering and its applications to photocatalysis, Ceram. Int. 40 (2014) 15523–15529.
[9] G. Li, Z. Lian, X. Li, Y. Xu, W. Wang, D. Zhang, F. Tian, H. Li, Ionothermal synthesis of black Ti 3+-doped single-crystal TiO 2 as an active photocatalyst for pollutant degradation and H 2 generation, J. Mater. Chem. A 3 (2015) 3748–3756.
[10] X. Chen, C. Burda, The electronic origin of the visible-light absorption properties of C-, N-and S-doped TiO_2 nanomaterials, J. Am. Chem. Soc. 130 (2008) 5018–5019.
[11] S. Klosek, D. Raftery, Visible light driven V-doped TiO2 photocatalyst and its photooxidation of ethanol, J. Phys. Chem. B 105 (2001) 2815–2819.
[12] A. Di Paola, E. Garcıa-López, S. Ikeda, G. Marcı, B. Ohtani, L. Palmisano, Photocatalytic degradation of organic compounds in aqueous systems by transition metal doped polycrystalline TiO 2, Catal. Today 75 (2002) 87–93.
[13] Q. Meng, T. Wang, E. Liu, X. Ma, Q. Ge, J. Gong, Understanding electronic and optical properties of anatase TiO 2 photocatalysts co-doped with nitrogen and transition metals, Phys. Chem. Chem. Phys. 15 (2013) 9549–9561.
[14] T. Ohno, M. Akiyoshi, T. Umebayashi, K. Asai, T. Mitsui, M. Matsumura, Preparation of S-doped TiO2 photocatalysts and their photocatalytic activities under visible light, Appl. Catal. A General 265 (2004) 115–121.
[15] T. Ohno, T. Mitsui, M. Matsumura, Photocatalytic activity of s-doped TiO2 photocatalyst under visible light, Chem. Lett. 32 (2003) 364–365.
[16] T. Umebayashi, T. Yamaki, S. Tanaka, K. Asai, Visible light-induced degradation of methylene blue on s-doped TiO2, Chem. Lett. 32 (2003) 330–331.
[17] R. Asahi, T. Morikawa, T. Ohwaki, K. Aoki, Y. Taga, Visible-light photocatalysis in nitrogen-doped titanium oxides, Science 293 (2001) 269–271.
[18] M. Maeda, T. Watanabe, Visible light photocatalysis of nitrogen-doped titanium oxide films prepared by plasma-enhanced chemical vapor deposition, J. Electrochem. Soc. 153 (2006) C186–C189.
[19] K. Yang, Y. Dai, B. Huang, Study of the nitrogen concentration influence on N-doped TiO2 anatase from first-principles calculations, J. Phys. Chem. C 111 (2007) 12086–12090.
[20] K. Yang, Y. Dai, B. Huang, Understanding photocatalytic activity of S-and P-doped TiO2 under visible light from first-principles, J. Phys. Chem. C 111 (2007) 18985–18994.
[21] H. Weng, X. Yang, J. Dong, H. Mizuseki, M. Kawasaki, Y. Kawazoe, Electronic structure and optical properties of the Co-doped anatase TiO 2 studied from first principles, Phys. Rev. B 69 (2004) 125219.
[22] R. Zhang, Q. Wang, J. Liang, Q. Li, J. Dai, W. Li, Optical properties of N and transition metal R (R= V, Cr, Mn, Fe, Co, Ni, Cu, and Zn) codoped anatase TiO 2, Phys. B Condens. Matter 407 (2012) 2709–2715.
[23] R. Zhang, Q. Wang, Q. Li, J. Dai, D. Huang, First-principle calculations on optical properties of C–N-doped and C–N-codoped anatase TiO 2, Phys. B Condens. Matter 406 (2011) 3417–3422.
[24] W. Qing, L. Ji-Feng, Z. Ren-Hui, L. Qiang, D. Jian-Feng, First-principle study on optical properties of N—La-codoped anatase TiO, Chin. Phys. B 22 (2013) 057801.
[25] C. Li, Y. Zhao, Y.Y. Gong, T. Wang, C.Q. Sun, Band gap engineering of early transition-metal-doped anatase TiO 2: first principles calculations, Phys. Chem. Chem. Phys. 16 (2014) 21446–21451.
[26] Y.F. Zhao, C. Li, S. Lu, R.X. Liu, J.Y. Hu, Y.Y. Gong, L.Y. Niu, Electronic, optical and photocatalytic behavior of Mn, N doped and co-doped TiO 2: experiment and

simulation, J. Solid State Chem. 235 (2016) 160–168.
[27] Y.F. Zhao, C. Li, S. Lu, L.J. Yan, Y.Y. Gong, L.Y. Niu, X.J. Liu, Effects of oxygen vacancy on 3d transition-metal doped anatase TiO 2: first principles calculations, Chem. Phys. Lett. 647 (2016) 36–41.
[28] Y. Fang, D. Cheng, W. Wu, Understanding electronic and optical properties of N–Sn codoped anatase TiO2, Comput. Mater. Sci. 85 (2014) 264–268.
[29] C.I.N. Morgade, G.F. Cabeza, Synergetic interplay between metal (Pt) and nonmetal (C) species in codoped TiO2: a DFT+U study, Comput. Mater. Sci. 111 (2016) 513–524.
[30] H.X. Zhu, J.M. Liu, Electronic and optical properties of C and Nb co-doped anatase TiO2, Comput. Mater. Sci. 85 (2014) 164–171.
[31] M. Lin, H. Chen, W. Chen, A. Nakaruk, P. Koshy, C. Sorrell, Effect of single-cation doping and codoping with Mn and Fe on the photocatalytic performance of TiO 2 thin films, Int. J. Hydrogen Energy 39 (2014) 21500–21511.
[32] J.P. Perdew, K. Burke, M. Ernzerhof, Generalized gradient approximation made simple, Phys. Rev. Lett. 77 (1996) 3865.
[33] W. Chen, P. Yuan, S. Zhang, Q. Sun, E. Liang, Y. Jia, Electronic properties of anatase TiO 2 doped by lanthanides: a DFT+ U study, Phys. B Condens. Matter 407 (2012) 1038–1043.
[34] R. Pentcheva, W.E. Pickett, Ionic relaxation contribution to the electronic reconstruction at the n-type LaAlO3/SrTiO3 interface, Phys. Rev. B Condens. Matter Mater. Phys. 78 (2008) 205106.
[35] J.K. Burdett, T. Hughbanks, G.J. Miller, J.W. Richardson Jr., J.V. Smith, Structural-electronic relationships in inorganic solids: powder neutron diffraction studies of the rutile and anatase polymorphs of titanium dioxide at 15 and 295 K, J. Am. Chem. Soc. 109 (1987) 3639–3646.
[36] A.D. Becke, K.E. Edgecombe, A simple measure of electron localization in atomic and molecular systems, J. Chem. Phys. 92 (1990) 5397–5403.
[37] F. Sen, Y. Qi, A. Alpas, Material transfer mechanisms between aluminum and fluorinated carbon interfaces, Acta Mater. 59 (2011) 2601–2614.
[38] J.J. Meléndez, Y.A. Zulueta, Y. Leyet, First-principles study of neutral defects in Fe-doped cubic barium titanate, Ceram. Int. 41 (2015) 1647–1656.
[39] G. Pan, Z. Xuejun, Z. Wenfang, W. Jing, L. Qingju, First-principle study on anatase TiO2 codoped with nitrogen and ytterbium, J. Semicond. 31 (2010) 032001.
[40] D.Y. Leung, X. Fu, C. Wang, M. Ni, M.K. Leung, X. Wang, X. Fu, Hydrogen production over titania-based photocatalysts, ChemSusChem 3 (2010) 681–694.
[41] J. Sato, N. Saito, H. Nishiyama, Y. Inoue, Photocatalytic activity for water decomposition of indates with octahedrally coordinated d10 configuration. I. Influences of preparation conditions on activity, J. Phys. Chem. B 107 (2003) 7965–7969.
[42] J. Sato, H. Kobayashi, K. Ikarashi, N. Saito, H. Nishiyama, Y. Inoue, Photocatalytic activity for water decomposition of RuO2-dispersed Zn2GeO4 with d10 configuration, J. Phys. Chem. B 108 (2004) 4369–4375.
[43] X. Chen, S.S. Mao, Synthesis of titanium dioxide (TiO2) nanomaterials, J. Nanosci. Nanotechnol. 6 (2006) 906–925.
[44] X. Chen, S.S. Mao, Titanium dioxide nanomaterials: synthesis, properties, modifications, and applications, Chem. Rev. 107 (2007) 2891–2959.
[45] X. Chen, L. Liu, F. Huang, Black titanium dioxide (TiO 2) nanomaterials, Chem. Soc. Rev. 44 (2015) 1861–1885.
[46] L. Zhao, X. Zhang, C. Fan, Z. Liang, P. Han, First-principles study on the structural, electronic and optical properties of BiOX (X=Cl, Br, I) crystals, Phys. B Condens. Matter 407 (2012) 3364–3370.
[47] H. Yan, Y. Guo, Q. Song, Y. Chen, First-principles study on electronic structure and optical properties of Cu-doped β-Ga2O3, Phys. B Condens. Matter 434 (2014) 181–184.
[48] N. Gao, C. Quan, Y. Ma, Y. Han, Z. Wu, W. Mao, J. Zhang, J. Yang, X.A. Li, W. Huang, Experimental and first principles investigation of the multiferroics BiFeO3 and Bi0.9Ca0.1FeO3: structure, electronic, optical and magnetic properties, Phys. B Condens. Matter 481 (2016) 45–52.
[49] J. Arul Mary, J. Judith Vijaya, M. Bououdina, L. John Kennedy, J.H. Daie, Y. Song, Investigation of structural, surface morphological, optical properties and first-principles study on electronic and magnetic properties of (Ce, Fe)-co doped ZnO, Phys. B Condens. Matter 456 (2015) 344–354.
[50] W. Wei, Y. Dai, M. Guo, L. Yu, B. Huang, Density functional characterization of the electronic structure and optical properties of N-doped, La-doped, and N/La-codoped SrTiO3, J. Phys. Chem. C 113 (2009) 15046–15050.